

Single-crystal elastic constants of ferromagnetic bcc Fe-based random alloys from first-principles theory

Hualei Zhang,¹ M. P. J. Punkkinen,^{1,2} Börje Johansson,^{1,3} Staffan Hertzman,⁴ and Levente Vitos^{1,3,5}

¹*Applied Materials Physics, Department of Materials Science and Engineering, Royal Institute of Technology, SE-10044 Stockholm, Sweden*

²*Department of Physics and Astronomy, University of Turku, FIN-20014 Turku, Finland*

³*Division of Materials Theory, Department of Physics and Materials Science, Uppsala University, P.O. Box 530, SE-75121 Uppsala, Sweden*

⁴*Department of Materials Science and Engineering, Outokumpu Stainless Research Foundation, Royal Institute of Technology, Stockholm SE-10044, Sweden*

⁵*Research Institute for Solid State Physics and Optics, P.O. Box 49, H-1525 Budapest, Hungary*

(Received 22 January 2010; revised manuscript received 7 April 2010; published 11 May 2010)

The elastic properties of ferromagnetic $\text{Fe}_{1-x}\text{M}_x$ ($M = \text{Al, Si, V, Cr, Mn, Co, Ni, and Rh}$; $0 \leq x \leq 0.1$) random alloys in the body-centered-cubic (bcc) crystallographic phase have been studied using the all-electron exact muffin-tin orbitals method in combination with the coherent-potential approximation. The theoretical lattice parameters and the single-crystal elastic constants agree well with the available experimental data. The most significant alloying effects are found for Al, Si, and Ni additions. All elements enlarge the lattice parameter and decrease the C_{11} , C_{12} , and C' elastic constants and the bulk modulus of bcc Fe. At the same time, C_{44} is found to increase with Al, Si, V, Cr, or Mn and remain nearly constant with Co, Ni, and Rh. Accordingly, the elastic anisotropy of bcc Fe increases with all alloying elements considered here. The calculated alloying effects on the single-crystal elastic constants are shown to originate from volume effects in combination with the peculiar electronic structure of bcc Fe.

DOI: [10.1103/PhysRevB.81.184105](https://doi.org/10.1103/PhysRevB.81.184105)

PACS number(s): 71.15.Nc, 71.20.Be, 62.20.D-, 81.05.Zx

I. INTRODUCTION

The stress-strain relation is often used to describe properties of solid materials.^{1–6} Elastic and plastic regimes can be distinguished using this relation. Within the elastic regime, the stress-strain relation is determined by the single-crystal and polycrystalline elastic parameters. The resistance of solid material to permanent or plastic deformation, on the other hand, is governed by dislocation motion and expressed via the yield stress or mechanical hardness. Empirical correlations exist between the elastic moduli and technologically important properties such as strength, hardness, and wear. One important example is the hardening mechanism in alloys, which arises from the disturbances in the lattice caused by the solute atoms in the matrix. The solid-solution hardening may be described by the classical Labusch-Nabarro model.^{7–9} Different solute atoms produce different effects on the volume and elastic constants of the host, which enables the design of alloys with novel properties. Therefore, it is of fundamental importance to describe and understand how the elastic parameters of engineering materials are influenced by the alloying elements.

Of particular interest in metallurgy is the effect of solute atoms on the elastic properties of ferromagnetic α -Fe. Significant efforts have been devoted to establish the elastic parameters of these alloys.^{3–6} The mechanism of substitutional solid-solution strengthening in iron was investigated on several single-crystal alloys.³ The effect of alloying elements on the Young's and shear modulus of iron was studied by Speich and co-workers⁴ and Ghosh and Olson.⁶ Many of these measurements, however, were performed on multiphase samples, and thus the obtained elastic parameters correspond to a

mixed phase rather than to a well-defined crystal structure. Nevertheless, today the available experimental data represent the most consistent starting point in modeling the mechanical properties of Fe-based alloys.

From theoretical side, most of the first-principles calculations focused on the chemical and magnetic properties,^{10–14} and only few studied the elastic properties of body-centered-cubic (bcc) Fe-based alloys.^{15–17} Recently, using the all-electron exact muffin-tin orbitals (EMTO) method^{18–20} in combination with the coherent-potential approximation (CPA),^{21,22} Zhang *et al.*¹⁶ demonstrated the composition dependence of the single crystal and polycrystalline elastic parameters of bcc Fe-Cr and Fe-Mg random alloys. It was found that alloying produces rather trivial variations in Fe-Mg but strongly nonlinear trends could be observed in Fe-Cr. Here, we extend the above *ab initio* study to the case of the ferromagnetic bcc $\text{Fe}_{1-x}\text{Al}_x$, $\text{Fe}_{1-x}\text{Si}_x$, $\text{Fe}_{1-x}\text{V}_x$, $\text{Fe}_{1-x}\text{Mn}_x$, $\text{Fe}_{1-x}\text{Co}_x$, $\text{Fe}_{1-x}\text{Ni}_x$, and $\text{Fe}_{1-x}\text{Rh}_x$ random alloys with $0 \leq x \leq 0.1$. These alloying elements were selected as representative simple metal (Al), insulator (Si), nonmagnetic (V and Rh), and magnetic transition metals (Mn, Co, and Ni), many of them being known as useful alloying elements in stainless steels. The present theoretical lattice parameters and single-crystal elastic constants agree reasonably well with the available experimental values. On the average, Al, Si, and Ni turn out to have the largest alloying effects on $C_{ij}(x)$. We show that all additions enlarge the lattice parameter and consequently decrease the single-crystal elastic constants C_{11} , C_{12} , and C' of bcc Fe. In spite of the increasing volume with alloying addition, the cubic shear modulus $C_{44}(x)$ exhibits slightly increasing trend with the concentration. This unusual alloying effect is due to the particular spin

density of states (DOS) of bcc Fe. The majority T_{2g} peak near the Fermi level gives a large negative contribution to the C_{44} of Fe. We demonstrate that all alloying additions which significantly alter the majority T_{2g} peak at the Fermi level lead to increasing $C_{44}(x)$.

At ambient conditions, the Fe-rich Fe-Al, Fe-Co, and Fe-Rh alloys adopt the body-centered-cubic (bcc) phase of α -Fe. The stability field of the α phase strongly depends on the alloying element and temperature. Around 400 °C approximately 21 atomic percent (at. %) Al can be dissolved in ferromagnetic α -Fe. The maximum solubility of Rh is ~ 19 at. % (at 600 °C) whereas Fe and Co form solid solution up to 77 at. % Co (at 100 °C).^{23,24} According to the x-ray diffraction and Mössbauer experiments,^{25–27} Fe-Si has the bcc phase below 10 at. % Si. The ferromagnetic Fe-V alloys also form a disordered bcc phase up to ~ 25 at. % V (around 300 °C).^{23,24} Within the high-temperature paramagnetic phase, both Fe-Cr and Fe-V alloys display complete solubility within the bcc phase. The solubility limit of Mn in ferromagnetic α -Fe is around 3 at. % (near room temperature) and that of Ni ~ 5.5 at. % (around 400 °C).^{23,24} Despite this low solubility of Mn and Ni in α -Fe, the present theoretical study is performed for Fe-based alloys containing up to 10 at. % alloying additions. By that we (a) try to minimize the numerical noises at low concentrations and (b) investigate some possible anomalies in the vicinity of the solubility limits within the two-phase region.

All binary systems considered in this study are treated as substitutional disordered ferromagnetic alloys with bcc underlying crystal structure. This approximation may be questioned at large concentrations, low temperatures and for alloy components with large size difference. However, in alloys with less than 10 at. % impurity atoms and near the room temperature, the random solid-solution model is expected to work reasonably well for the total energies.^{17,28,29} The local lattice relaxations around large impurity atoms, on the other hand, could strongly influence the energetics and thus the computed physical parameters. This effect will be scrutinized in details here.

The rest of the paper is divided in four main sections. The theoretical tool is presented in Sec. II. Here we give a brief overview of the EMTO electronic structure and total-energy method and the most important details of the numerical calculations. In order to establish the accuracy of our theoretical approach for the elastic properties of disordered Fe-based alloys, in Sec. III we compare some EMTO results to those obtained using the projector augmented wave (PAW) method as implemented in Vienna *ab initio* simulation package^{30–33} (the latter results will be referred to as VASP). In this section, we also discuss the accuracy of the single-site coherent-potential approximation as implemented in the EMTO method.²⁰ The results obtained for the single-crystal elastic properties, bulk moduli, and elastic anisotropies of Fe-based alloys are presented and discussed in Sec. IV. Here, for comparison, we also quote our former results obtained for $\text{Fe}_{1-x}\text{Cr}_x$. The atomic-level mechanisms behind the calculated trends are discussed in Sec. V. Here, first we single out the volume effect in the single-crystal elastic constants. Then we investigate the electronic structure of ferromagnetic Fe and $\text{Fe}_{0.95}\text{M}_{0.05}$ alloys ($M = \text{Al, Si, V, Cr, Mn, Co, Ni, and Rh}$)

in the ideal bcc structure and in a distorted structure used to calculate the C_{44} elastic constant.

II. COMPUTATIONAL METHOD

A. Total-energy calculations

The present calculations are based on the density-functional theory³⁴ formulated within the Perdew-Burke-Ernzerhof (PBE) generalized gradient approximation for the exchange-correlation functional.³⁵ The Kohn-Sham equations³⁶ are solved using the EMTO method.^{18,19} The substitutional disorder is treated within CPA.^{19,21,22} From the self-consistent charge density, the total energy is calculated by the full charge-density technique.^{19,37}

The EMTO method is an improved screened Korringa-Kohn-Rostoker (KKR) method,¹⁸ where the one-electron potential is represented by optimized overlapping muffin-tin potential spheres. By using the overlapping spheres, one describes more accurately the exact crystal potential, compared to the conventional muffin-tin or nonoverlapping approach.¹⁹ The present implementation is based on a scalar-relativistic Green's-function technique. Further information of the EMTO method and its self-consistent implementation can be found in Refs. 18, 19, 38, and 39. The EMTO approach ensures the accuracy needed for the calculations of the anisotropic lattice distortions in random alloys. The method has been applied successfully in the *ab initio* study of the thermophysical properties of random Fe-based alloys,^{16,17,40–45} simple and transition-metal alloys,^{19,46–50} as well as complex oxide solid solutions.^{51–54}

B. Numerical details

The elastic properties of single crystals are described by the elements C_{ij} of the elasticity tensor. There are three independent elastic constants for a cubic lattice: C_{11} , C_{12} , and C_{44} , and they are connected to the tetragonal shear modulus $C' = (C_{11} - C_{12})/2$ and the bulk modulus $B = (C_{11} + 2C_{12})/3$. Dynamical (mechanical) stability requires that $C_{44} > 0$, $C' > 0$, and $B > 0$.⁵⁵ The elastic anisotropy is commonly described by the parameters introduced by Every⁵⁶ and Zener.⁵⁷ The Every parameter is defined as $A_E = (C_{11} - C_{12} - 2C_{44}) / (C_{11} - C_{44})$ and the Zener ratio as $A_Z = 2C_{44} / (C_{11} - C_{12})$. For an isotropic cubic crystal (i.e., $C_{11} - C_{12} = 2C_{44}$), we have $A_E = 0$ and $A_Z = 1$.

The cubic elastic constants of the ferromagnetic bcc $\text{Fe}_{1-x}\text{M}_x$ ($M = \text{Al, Si, V, Cr, Mn, Co, Ni, and Rh}$) random alloys were calculated as a function of the chemical composition for $0 \leq x \leq 0.1$. At each concentration x , the theoretical equilibrium lattice parameter $a(x)$ and bulk modulus $B(x)$ were derived from an exponential Morse-type function⁵⁸ fitted to the *ab initio* total energies calculated for seven different atomic volumes. The two cubic shear moduli $C'(x)$ and $C_{44}(x)$ were computed using the volume-conserving orthorhombic and monoclinic deformations as described in Ref. 39.

For an $\text{Fe}_{1-x}\text{M}_x$ solid solution, the size and bulk-modulus misfit parameters are defined as

$$\varepsilon_Y = \frac{1}{Y} \frac{dY}{dx}, \quad (1)$$

where Y stands for the Burgers vector b for the size misfit (ε_b) and for the bulk modulus B for the bulk-modulus misfit (ε_B). Numerically, ε_b and ε_B were calculated from the concentration-dependent lattice parameter $a(x)$ and bulk modulus $B(x)$ by taking the average slopes up to 5 at. % ($x=0.05$) impurity concentrations.

The one-electron equations were solved within the scalar-relativistic and soft-core approximations. The Green's function was calculated for 16 complex energy points distributed exponentially on a semicircular contour. In the EMTO basis set, we included s , p , d , and f orbitals ($l_{\max}=3$), and in the one-center expansion of the full charge density $l_{\max}^h=8$ was used.³⁹ All calculations were performed for ferromagnetic bcc alloys. The total energy was evaluated by the shape function technique. To obtain the accuracy needed for the calculation of elastic constants, we used about 20 000–25 000 uniformly distributed k points in the irreducible wedge of the monoclinic and orthorhombic Brillouin zones. For the density of states, approximately 60 000–80 000 k points were used. The electrostatic correction to the single-site coherent-potential approximation was described using the screened impurity model⁵⁹ with screening parameter of 0.6. For all alloy components, the potential sphere radii were chosen to be equal to the corresponding average atomic sphere radius. All calculations were performed for static lattice (neglecting the phonon contributions).

III. ASSESSING THE ACCURACY OF THE THEORETICAL TOOL

The most straightforward way to model a random alloy is to carry out accurate calculations for large supercells (SCs) with randomly distributed alloy components or for special quasirandom structures.^{60,61} However, in alloys containing only a few percent impurity atoms, the above approaches become very expensive. The computational efforts may be reduced by employing the coherent-potential approximation,^{21,22,39} which is the most powerful approach within the alloy theory. Unfortunately, due to its single-site nature, the CPA cannot be combined with accurate techniques such as the full-potential methods. Because of that, most of the existing CPA methods are based on conventional muffin-tin or atomic sphere approximations. The EMTO-CPA method, on the other hand, is an improved muffin-tin CPA approach, which goes beyond the standard muffin-tin approximation by employing optimized overlapping muffin-tin potentials. In this section, we assess the accuracy of the EMTO-CPA approach by comparing the EMTO and VASP results obtained for supercells (Sec. III A) and the CPA and the supercells results (Sec. III B).

A. EMTO versus VASP

In order to establish the accuracy of the EMTO method for ferromagnetic Fe-based alloys, we carried out additional total-energy calculations using the VASP,^{30–33} which is a commonly accepted accurate density-functional total-energy

method based on the projector-augmented wave approach.^{62,63} For the present comparison, we decided to use a 16-atom supercell formed by $2 \times 2 \times 2$ bcc unit cells. In these VASP calculations, the number of k points in the irreducible wedge of the Brillouin zone was set to 120 and 450 eV energy cutoff for plane waves was used. These values lead to convergence in the total energy within about 1 meV.

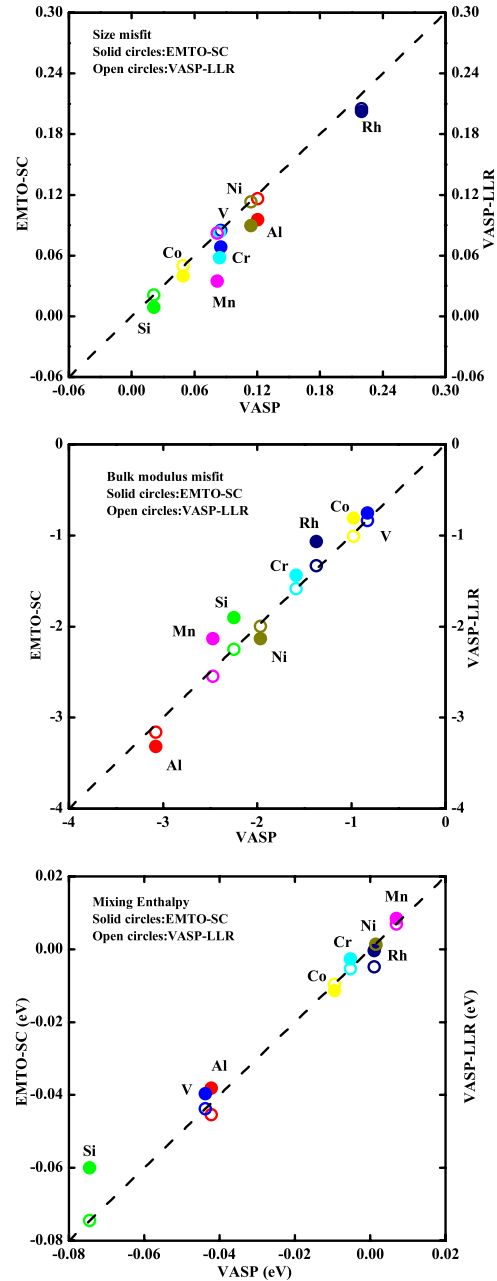


FIG. 1. (Color online) Comparison of the size misfit (upper panel) and bulk-modulus misfit (middle panel) parameters, and mixing enthalpies per atom (lower panel) of ferromagnetic bcc Fe_{15}M_1 ($M=\text{Al, Si, V, Cr, Mn, Co, Ni, and Rh}$) alloys calculated using the EMTO and VASP methods (EMTO-SC, solid circles) in combination with the supercell technique. The effect of the local lattice relaxation, as calculated using the VASP method, is also shown (VASP-LLR, open circles).

TABLE I. The effect of the local lattice relaxation around the impurity atoms in the ferromagnetic bcc $\text{Fe}_{15}M_1$ ($M=\text{Al, Si, V, Cr, Mn, Co, Ni, and Rh}$) alloys on the nearest-neighbor distance (Δd) and the total energy (ΔE , per impurity atom) as calculated using the VASP method.

	Fe-Al	Fe-Si	Fe-V	Fe-Cr	Fe-Mn	Fe-Co	Fe-Ni	Fe-Rh
Δd (Å)	+0.028	0.001	+0.002	-0.005	+0.002	-0.002	+0.007	+0.035
ΔE (eV)	-0.051	0.000	0.000	-0.001	0.000	-0.001	-0.002	-0.093

For each Fe- M binary system, the SC consisted of 15 Fe atoms and one impurity atom (M). In order to be able to make a direct comparison between the corresponding EMTO and VASP results, we repeated all supercell calculations using the EMTO method as well. These EMTO results are referred to as the EMTO-SC values. First, both the VASP and the EMTO-SC results were obtained for rigid (unrelaxed) supercells, neglecting the effect of the local lattice distortions around the impurity atoms. For comparison, we consider the size and bulk-modulus misfit parameters calculated by the two methods. Since the supercells correspond to 6.25 at. % doping, these SC misfit parameters were computed according to

$$\varepsilon_Y = \frac{1}{Y_0} \frac{Y_{\text{SC}} - Y_0}{0.0625}, \quad (2)$$

where Y stands either for the lattice parameter (for ε_b) or the bulk modulus (for ε_B), and Y_{SC} and Y_0 are the corresponding values for the $\text{Fe}_{15}M_1$ supercell and for pure bcc Fe, respectively.

In addition to the misfit parameters, we also compare the EMTO and VASP mixing enthalpies per atom. As standard states, we used the ferromagnetic bcc Fe in combination with face-centered-cubic (fcc) Al, Si in diamond structure, bcc V, antiferromagnetic Cr in CsCl structure, hypothetical ferromagnetic bcc Mn, ferromagnetic Co in hexagonal-close-packed structure (with the experimental hexagonal lattice parameter of 1.62), ferromagnetic fcc Ni, and fcc Rh.

Figure 1 displays the EMTO-SC misfit parameters and mixing enthalpies as a function of the corresponding (unrelaxed) VASP values. A perfect agreement between the two sets of results would correspond to solid circles lying on the dashed line with slope 1. In general, the agreement between the two sets of theoretical data is good for all parameters. The mean absolute deviations between the EMTO-SC and VASP ε_b and ε_B values are 0.02 and 0.3, respectively. For the size misfit, a somewhat larger difference is found for Fe-Mn. This deviation may be ascribed to the magnetic transition near the equilibrium volume. Namely, according to our calculations, the magnetic coupling between Fe and Mn changes from ferromagnetic to antiferromagnetic with increasing volume, which makes the accurate determination of the equilibrium properties rather difficult. At this point, we should point out that a ~ 0.02 difference between the EMTO-SC and VASP ε_b values corresponds to less than 0.002 Å error in the EMTO equilibrium Wigner-Seitz radius. Except for Si, the EMTO-SC and VASP mixing enthalpies are also in line with each other. The ~ 14 meV deviation in the mixing enthalpy of Fe-Si most likely is due to the

EMTO error for the diamond structure, where so-called empty spheres need to be included for acceptable potential overlaps.³⁹

Using the VASP technique, we also investigated the effect of local lattice relaxation (LLR) around the impurities on the misfit parameters and mixing enthalpy. The corresponding VASP results are shown by open symbol in Fig. 1 (VASP-LLR). For ε_b and ε_B , there is an almost perfect agreement between the unrelaxed (VASP) and relaxed (VASP-LLR) values, meaning that the misfit parameters are not significantly affected by the LLR. The largest LLR effects on ε_b and ε_B are seen for Al and Rh. In the case of the mixing enthalpy, however, the LLR turns out to be more important. In particular, we find that the LLR changes the sign of the mixing enthalpy of Fe-Rh.

The relatively small impact of the LLR can be understood if we have a look to the effect of the LLR on the nearest-neighbor distance around the impurity atoms (Δd) and the total energy (ΔE) (Table I). For all binaries considered here, Δd is calculated to be below 1.4% of the nearest-neighbor distance in pure bcc Fe is (2.452 Å). The largest relaxation effects are obtained for Al and Rh, which are due to the 12% and 5% atomic radius difference between bcc Fe and fcc Al and Rh. For the rest of the elements, both Δd and ΔE are very small.

Comparing the EMTO-SC and VASP-LLR values to the VASP values from Fig. 1, we find that the EMTO-SC results deviate more significantly from the VASP results than the effect of the LLR. Although both methods employed here suffer from some intrinsic numerical errors, the present deviations most likely are due to the muffin-tin and spherical cell approximations used in the EMTO approach.^{18,19,39} Therefore, we consider the 0.02 and 0.3 mean absolute deviations between the EMTO-SC and VASP ε_b and ε_B values, respectively, as the error bars associated with the present EMTO calculations. All EMTO results for the elastic properties from Sec. IV will be analyzed by taking into account these error bars.

B. Coherent-potential approximation versus supercell approach

We use the coherent-potential approximation to describe the random solid-solution model of the Fe- M alloys. There are several approximations involved in the CPA. It neglects both the short-range order and the local lattice relaxation effects. In addition, being a single-site approximation to the impurity problem, the electrostatic interactions around the impurity atoms are not accounted for either. Several corrections have been worked out which improve the original CPA

and extend its application field. It is beyond the scope of the present work to discuss these corrections or to make attempts to justify one or the other.

Our aim is to describe the elastic properties of Fe-rich alloys as a function of chemical composition. In order to make sure that the employed CPA along with all inherent approximations is able to describe properly the alloying effects on the elastic parameters, we carry out a test by contrasting the CPA approach with the formally exact (within the numerical errors discussed above) SC approach. Namely, we compare the volume and bulk-modulus misfit parameters for the considered ferromagnetic bcc Fe-based alloys calculated by CPA and SC techniques. In these CPA calculations, the Fe- M system was described as a random bcc $\text{Fe}_{0.9375}M_{0.0625}$ alloy whereas in the SC calculations the 16-atom supercell containing 15 Fe and one M was considered.

The results of the CPA versus SC test are shown in Fig. 2. The almost perfect agreement between the two sets of size misfit data (upper panel) is slightly destroyed for the bulk-modulus misfit (middle panel). However, even for ε_B , the deviations are within the numerical accuracy of our technique. For Fe-Si, EMTO-CPA yields small positive ε_b (~ 0.028) whereas the EMTO-SC value is 0.009. On the other hand, the EMTO-CPA result turns out to be rather close to the corresponding VASP value of 0.021.

Although the general trend for the mixing enthalpies is well captured by the single-site approximation, we can observe sizable differences in the case of V, Cr, Ni, and Rh (Fig. 2, lower panel). In this comparison, we should realize however that the 16-atom supercell is a relatively low-order approximation for the random system and thus one cannot expect a perfect agreement between the two sets of data. Furthermore, in the present CPA calculations, we used a fixed screening parameter.⁵⁹ For more accurate CPA mixing enthalpies, one should determine the concentration- and structure-dependent screening parameter using large supercells. This is an enormous task and points beyond the scope of the paper. On the other hand, we recall that the elastic properties of random alloys depend only weakly on the screening parameter,^{39,48} and thus using a fixed screening parameter is expected to introduce negligible errors in the calculated C_{ij} values.

The generally good agreement between EMTO-SC and EMTO-CPA misfit parameters from Fig. 2 indicates that at least up to 6.25 at. % impurity concentration the effect of alloying on the bulk parameters is properly described by our single-site EMTO-CPA approach. Hence, in Sec. IV, we present and discuss theoretical results obtained exclusively with the EMTO-CPA approach (for simplicity, these results will be referred to as the EMTO values).

IV. ELASTIC PROPERTIES OF FERROMAGNETIC bcc $\text{Fe}_{1-x}M_x$ ($M=\text{Al, Si, V, Cr, Mn, Co, Ni, and Rh}$) RANDOM ALLOYS WITH $0 \leq x \leq 0.1$

A. Lattice parameters

The calculated bcc lattice parameters $a(x)$ of $\text{Fe}_{1-x}M_x$ alloys are displayed in Fig. 3 and listed in Table II as a function of solute concentration x . In Fig. 3, we also included the

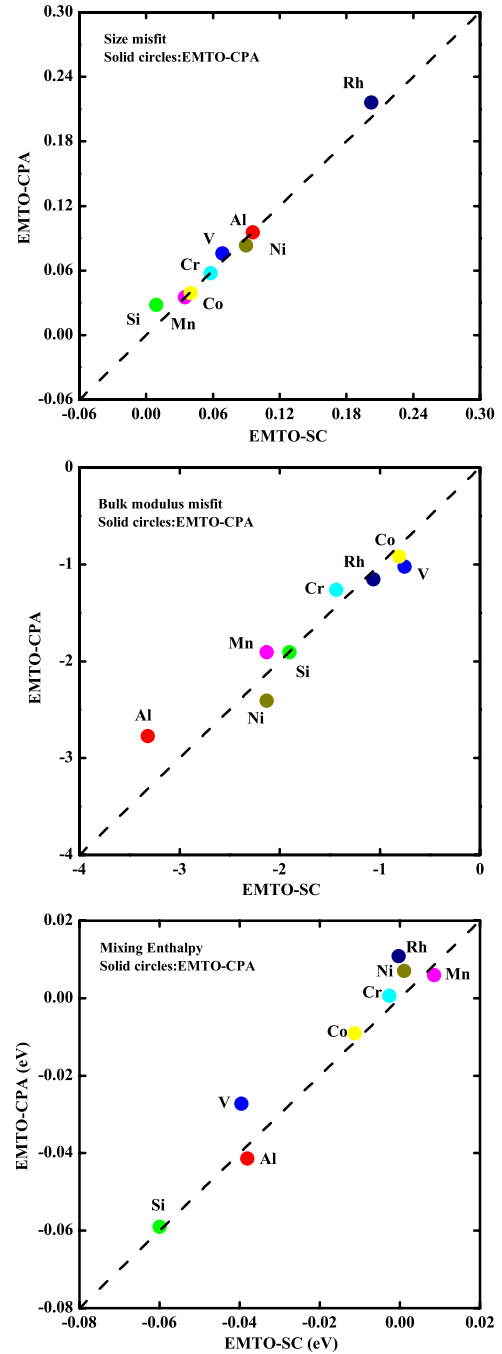


FIG. 2. (Color online) Comparison of the size misfit (upper panel) and bulk-modulus misfit (middle panel) parameters, and mixing enthalpies (lower panel) of the ferromagnetic bcc $\text{Fe}_{0.9375}M_{0.0625}$ ($M=\text{Al, Si, V, Cr, Mn, Co, Ni, and Rh}$) alloys calculated using the supercell (EMTO-SC) and the CPA (EMTO-CPA) approaches.

available experimental data^{25,64–73} and the theoretical results for Fe-Si system obtained using an *ab initio* KKR-CPA method.⁷⁴

For most of the binary alloys from Fig. 3, the present theoretical lattice parameters increase monotonously with the solute concentration. However, the small positive slopes for Fe-Mn and Fe-Cr at low- x values are gradually reduced turning negative at large x . For these two systems as well as for

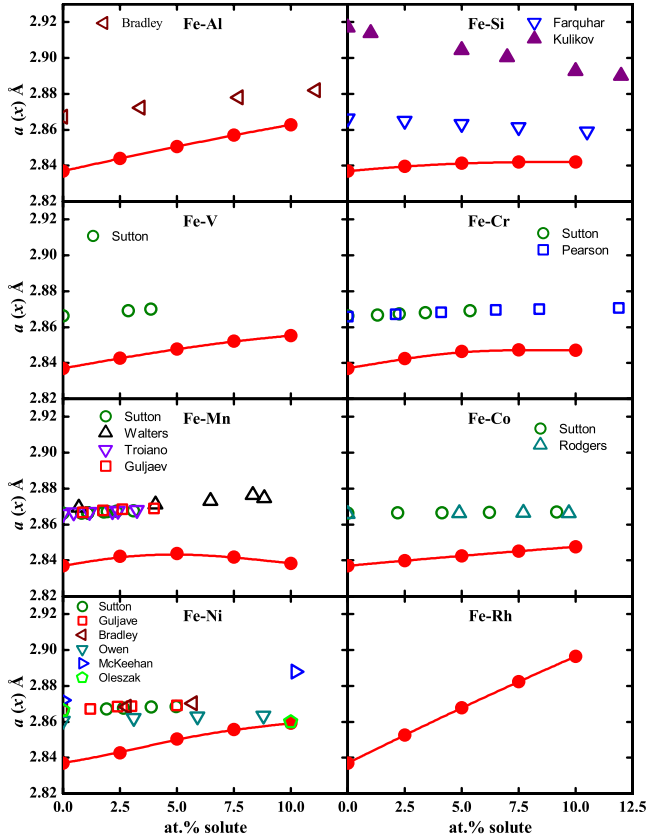


FIG. 3. (Color online) Theoretical (present results, solid circles connected with lines) and experimental (Refs. 25 and 64–73, open symbols) lattice parameters of ferromagnetic bcc $\text{Fe}_{1-x}\text{M}_x$ ($M=\text{Al}$, Si , V , Cr , Mn , Co , Ni , and Rh ; $0 \leq x \leq 0.1$) random alloys. For comparison, the former theoretical results for Fe-Si (solid triangles) are also shown (Ref. 74).

Fe-Ni and to some extent also for Fe-Si, the EMTO $a(x)$ trends clearly deviate from the linear behavior. As expected, the largest volume effects are obtained for Al and Rh doping whereas Si addition leaves the lattice parameter of Fe almost intact. A former theoretical study of the electronic and magnetic properties of disordered bcc Fe-Si alloys with less than 25 at. % Si, based on *ab initio* KKR-CPA approach,^{74,75} also calculated weak composition dependence for the lattice parameter of Fe-Si. However, this KKR-CPA study predicted slightly decreasing $a(x)$ for $\text{Fe}_{1-x}\text{Si}_x$ with increasing x .^{74,75} In contrast, here we find that both EMTO and VASP methods yield small but positive slopes for $a(x)$ with Si addition. We point out that our finding for the lattice parameter of Fe-Si alloys is consistent with the negative bulk-modulus misfit obtained for Fe-Si (Figs. 1 and 2), which is in line with the experimental data.⁷⁶

In general, the agreement in Fig. 3 between the present theoretical results and the experimental data is satisfactory. It is well known that the PBE density-functional approximation³⁵ underestimates the volume of pure Fe and only part of this error is removed by the lattice vibration (neglected in the present study). Nevertheless, the observed concentration dependences of the lattice parameters of Fe- M alloys are well captured by the theory. In particular, the local maximum for Fe-Cr is reproduced by the theory, although

with significantly larger positive slope at low- x values. The theoretical local maximum for the lattice parameter of Fe-Mn, on the other hand, is missing from the experimental data. However, the calculated maximum as well as the negative $a(x)$ slope for Fe-Mn is located well outside the stability field of the bcc Fe-Mn alloys, indicating that the quoted experimental data refers to a mixed phase rather than to the pure α phase.⁶⁹

In Fig. 4, we compare the present theoretical misfit parameters for the lattice constants (size misfit) to the experimental values from Ref. 6. The theoretical results from Fig. 4 were derived from the average slopes between 0 and 5 at. % of the EMTO $a(x)$ functions (Fig. 3), as described in Sec. II B. We find that the experimentally observed alloying effects on the lattice parameter of Fe-based alloys are well-captured by the EMTO method combined with the CPA technique.⁶ But we also notice that EMTO systematically overestimates the relative changes in the lattice parameters. The deviation ranges between ~ 0.03 obtained for Fe-Mn and ~ 0.11 calculated for Fe-Rh. In the case of Fe-Si, the above deviation is large enough to turn the experimental negative size misfit to a small positive value.

It seems that the overestimation of the size misfit by the theory has a rather universal character for the present Fe-based alloys. The almost constant deviation between theoretical and experimental ε_b as going from Al to Ni, and the fact that no similar consistent deviations were obtained for the Al-based alloys^{50,77} suggest that part of the discrepancies from Fig. 4 should be due to the fundamental density-functional error present in Fe and Fe-rich alloys. The PBE functional is known to underestimate (overestimate) the equilibrium volumes of V, Cr, and Fe (Si, Rh), and predict accurate volumes for Al, Co, and Ni.^{78–80} As an example, we consider the case of Fe-Rh. Static (0 K) PBE calculations underestimate the equilibrium Wigner-Seitz radius of bcc Fe by ~ 0.014 Å and overestimate that of fcc Rh by ~ 0.020 Å.⁷⁸ This means that in Fe-Rh alloys, the PBE error gives an additional positive slope of $(\Delta a/\Delta x/a)_{\text{PBE}} \approx 0.03$. Similarly, we find that the PBE error increases the theoretical size misfit of the Fe-Al, Fe-Si, Fe-Co, and Fe-Ni alloys. Although, this error cannot completely explain the deviations seen in Fig. 4, it clearly gives a positive contribution to the theoretical size misfit parameters. The accuracy of PBE for the solute atom in ferromagnetic bcc Fe matrix may be different from that for the pure metal. Nevertheless, for a more accurate theoretical estimate of the size effects better density functionals are required.

B. Single-crystal elastic constants

Next, we present our theoretical results for the single-crystal elastic constants of ferromagnetic bcc $\text{Fe}_{1-x}\text{M}_x$ ($M=\text{Al}$, Si , V , Cr , Mn , Co , Ni , and Rh ; $0 \leq x \leq 0.1$) alloys. For each solute concentration x , the single-crystal elastic constants were calculated at the corresponding theoretical equilibrium lattice parameter $a(x)$ (Fig. 3). Results for $C_{11}(x)$, $C_{12}(x)$, $C'(x)$, and $C_{44}(x)$ are plotted in Fig. 5 and listed in Table II.

The accuracy of the theoretical $C_{ij}(x)$ values can be estimated by comparing them with the experimental values

TABLE II. Theoretical (EMTO) equilibrium lattice parameters $a(x)$ (in Å) and single-crystal elastic constants $C_{ij}(x)$ (in GPa) calculated for the ferromagnetic bcc $\text{Fe}_{1-x}M_x$ ($M=\text{Al, Si, V, Cr, Mn, Co, Ni, and Rh}$; $0 \leq x \leq 0.1$) random alloys. For pure Fe, the corresponding values are $a(0)=2.837$ Å, $C_{11}(0)=297.83$ GPa, $C_{12}(0)=141.89$ GPa, $C'(0)=77.97$ GPa, and $C_{44}(0)=106.73$ GPa (Ref. 16).

x	$a(x)$	$C_{11}(x)$	$C_{12}(x)$	$C'(x)$	$C_{44}(x)$	$a(x)$	$C_{11}(x)$	$C_{12}(x)$	$C'(x)$	$C_{44}(x)$
Fe-Al						Fe-Si				
0.025	2.844	270.71	128.03	71.34	108.77	2.840	277.10	130.25	73.43	110.61
0.05	2.851	253.56	119.87	66.84	111.34	2.841	267.12	125.54	70.79	115.15
0.075	2.857	240.98	114.34	63.32	114.76	2.842	262.15	124.60	68.78	119.94
0.1	2.863	233.46	111.98	60.74	118.67	2.842	260.07	126.96	66.55	124.03
Fe-V						Fe-Cr				
0.025	2.843	290.15	136.78	76.69	106.80	2.843	284.17	131.51	76.33	108.56
0.05	2.848	286.15	132.92	76.61	107.86	2.846	279.96	126.87	76.54	112.83
0.075	2.852	285.36	130.37	77.49	109.66	2.847	283.52	127.19	78.16	117.51
0.1	2.855	288.91	130.36	79.27	111.98	2.847	287.75	127.92	79.91	120.71
Fe-Mn						Fe-Co				
0.025	2.842	276.15	126.29	74.93	109.75	2.840	289.75	137.50	76.12	106.05
0.05	2.844	269.24	120.37	74.44	114.73	2.842	284.07	134.03	75.02	106.15
0.075	2.842	275.24	122.66	76.29	118.35	2.845	280.10	131.68	74.21	106.90
0.1	2.838	285.53	129.91	77.81	120.90	2.848	277.06	130.25	73.41	108.17
Fe-Ni						Fe-Rh				
0.025	2.843	275.89	127.06	74.42	105.17	2.853	284.66	138.47	73.10	104.64
0.05	2.850	255.29	117.29	69.00	104.59	2.868	274.50	135.51	69.50	104.36
0.075	2.856	240.47	110.09	65.19	105.69	2.882	266.87	133.37	66.75	104.95
0.1	2.859	231.78	107.46	62.16	108.17	2.897	259.60	130.55	64.52	106.02

available for Fe-Al with 3.97 and 9.65 at. % Al (Ref. 81) and for pure Fe.⁸² Theory turns out to be able to trace the experimental concentration dependences of the elastic constants upon Al addition to bcc Fe. In particular, the negative trends for $C_{11}(x)$ and $C_{12}(x)$ and the weak positive trend of $C_{44}(x)$ are accurately reproduced by the present theory. In lack of other single-crystal experimental data, we turn to discuss the trends from Fig. 5. Further comparison between theory and experiment will be presented in the case of the bulk modulus (Sec. IV C).

For all binaries considered here, the theoretical elastic constants $C_{11}(x)$, $C_{12}(x)$, and $C'(x)$ decrease with x for solute

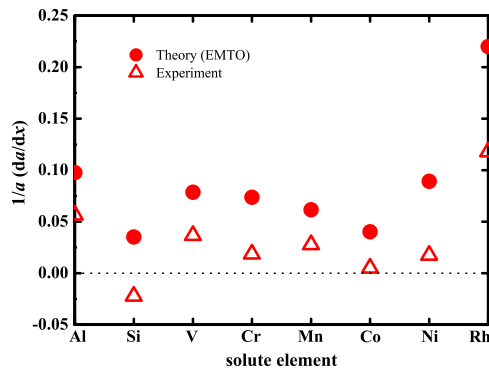


FIG. 4. (Color online) Theoretical (present results, solid circles) and experimental (Ref. 6, open symbols) relative changes in the lattice parameter for $\text{Fe}_{1-x}M_x$ ($M=\text{Al, Si, V, Cr, Mn, Co, Ni, and Rh}$; $0 \leq x \leq 0.05$) random binary alloys.

concentrations below 5 at. %. When 5 at. % Al, Si, Mn, or Ni is added to bcc Fe, the C_{11} elastic parameter of Fe is reduced by 14.9%, 10.3%, 9.6%, and 14.3%, respectively. The corresponding changes with V, Cr, and Co additions are significantly smaller: -3.9%, -6.0%, and -4.6%, respectively. Rhodium produces an intermediate effect on C_{11} : 5 at. % Rh changes C_{11} of Fe by -7.8%. Notice that these changes correspond to 5 at. % solute concentration, and might differ from the average slopes below $x=0.05$. The $C_{11}(x)$ curves for Fe-V, Fe-Cr, and Fe-Mn are nonmonotonous, exhibiting local minima around 7.5 at. % V, 5 at. % Cr, and 5 at. % Mn.

Similar to $C_{11}(x)$, C_{12} of $\text{Fe}_{0.95}\text{Al}_{0.05}$, $\text{Fe}_{0.95}\text{Si}_{0.05}$, $\text{Fe}_{0.95}\text{Mn}_{0.05}$, and $\text{Fe}_{0.95}\text{Ni}_{0.05}$ are smaller by about 15.5%, 11.5%, 15.2%, and 17.3%, respectively, than that of pure Fe. The effects of V, Co, and Rh are -6.3%, -5.5%, and -4.5%. However, C_{12} turns out to be more sensitive to Cr addition than C_{11} : 5 at. % Cr decreases C_{12} of bcc Fe by more than 10%. There are local minima also for $C_{12}(x)$: at 7.5 at. % Si and V, and at 5 at. % Cr and Mn.

Since all alloying additions decrease C_{11} and C_{12} , the absolute changes in $C'=(C_{11}-C_{12})/2$ are expected to be small. However, since for pure Fe $C_{11} \approx 2.1C_{12}$, similar relative changes in C_{11} and C_{12} (up to 5 at. % solute concentrations) result in decreasing C' for all binaries considered. Indeed, we find that C' drops by approximately 14.3%, 9.2%, 1.7%, 1.8%, 4.5%, 3.8%, 11.5%, and 10.9% when 5 at. % Al, Si, V, Cr, Mn, Co, Ni, or Rh is added to bcc Fe. That is, all additions lower the tetragonal shear constant of bcc Fe. The $C'(x)$ curves for Fe-V and Fe-Mn show local minima near

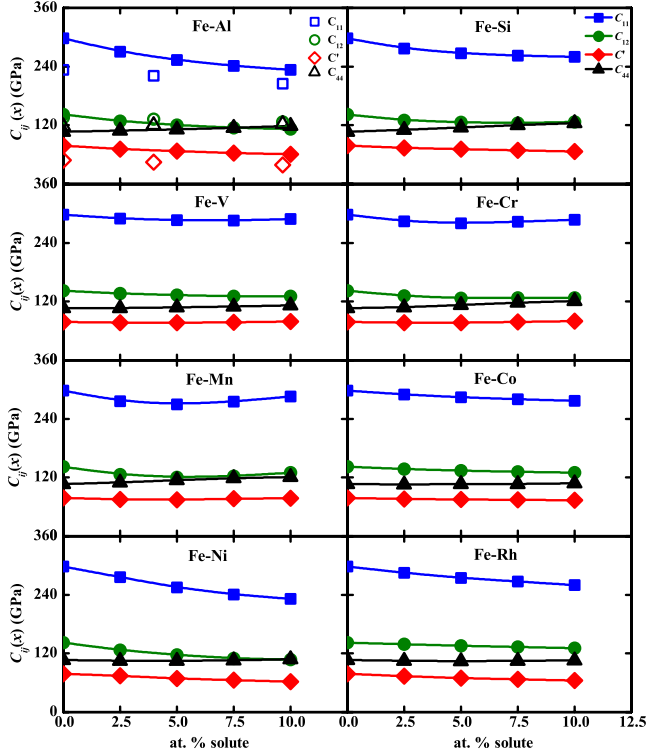


FIG. 5. (Color online) Theoretical (present results, solid symbols connected with lines) single-crystal elastic constants of ferromagnetic bcc $Fe_{1-x}M_x$ ($M=Al, Si, V, Cr, Mn, Co, Ni,$ and $Rh; 0 \leq x \leq 0.1$) random alloys. For comparison, the experimental data (open symbols) for $Fe_{1-x}Al_x$ are also shown ($x=0.0397, 0.0965$ from Ref. 81 and $x=0$ from Ref. 82).

5 at. % impurity concentration, and that of Fe-Cr has minimum at 2.5 at. % Cr. It is notable that with 10 at. % V or Cr (Mn) addition, the calculated $C'(0.1)$ exceeds (reaches) the C' of pure Fe (77.97 GPa).

Compared to the above complex concentration dependences of $C_{11}(x), C_{12}(x),$ and $C'(x),$ the calculated $C_{44}(x)$ curves show nearly linear and relatively weak variations with composition (Fig. 5). The relative changes in $C_{44}(x)$ upon 5 at. % solute addition are 4.3%, 7.9%, 1.1%, 5.7%, 7.5%, -0.5%, -2.0%, and -2.2% for Al, Si, V, Cr, Mn, Co, Ni, and Rh, respectively. The largest effect on $C_{44}(x)$ is produced by 10 at. % addition of Si (16.2%), followed by Mn (13.3%), Cr (13.1%), and Al (11.2%). Cobalt, nickel, and rhodium additions lead to weak local minima in $C_{44}(x)$ at 2.5 at. %

Co and Ni and 5 at. % Rh. It is interesting that $C_{44}(x)$ of Fe-Co, Fe-Ni, and Fe-Rh remain close (within 1.3%) to that of pure Fe even for 10 at. % doping. Furthermore, Al, Si, V, Cr, and Mn increase the C_{44} cubic shear modulus of Fe. This is rather surprising since all additions increase the equilibrium volume of bcc Fe (see Sec. V).

In summary, at 5 at. % solute concentration, Al, Si, Mn, and Ni are found to reduce strongly (between 9.6% and 17.3%) the C_{11} and C_{12} elastic constants of ferromagnetic bcc Fe. On the other hand, the two cubic shear moduli show different behavior upon alloying. Namely, C' is significantly decreased (9.2–14.3 %) by Al, Si, Ni, and Rh whereas C_{44} increases (4.3–7.9 %) with Al, Si, Cr, and Mn. On the average, Al, Si, and Ni yield the largest alloying effects on the single-crystal elastic constants of bcc Fe.

C. Bulk modulus

Our theoretical results for the bulk modulus $B(x)$ of ferromagnetic bcc $Fe_{1-x}M_x$ ($M=Al, Si, V, Cr, Mn, Co, Ni,$ and $Rh; 0 \leq x \leq 0.1$) alloys are presented in Table III and compared to the available experimental data^{4,76,81} in Fig. 6. At concentrations $x \leq 0.05,$ theory predicts a negative slope for $B(x)$ for all binaries considered here. This is consistent with our finding from Fig. 4, namely, that all elements considered here increase the equilibrium volume of ferromagnetic bcc Fe. Aluminum and nickel additions are calculated to yield the largest alloying effects in $B(x)$ (see also Fig. 2). The theoretical bulk moduli of Al, Co, Ni, and Rh-doped Fe decrease monotonously with alloying, and local minima in $B(x)$ can be observed around 7.5 at. % Si, 7.5 at. % V, 5 at. % Cr, and 5 at. % Mn.

No experimental bulk-moduli data are available for Fe-V alloys. The experimental bulk moduli for Fe-Al with 3.97 and 9.65 at. % Al may be calculated from the measured single-crystal elastic constants (Fig. 6).⁸¹ Combining those values with the room-temperature experimental bulk modulus of pure Fe (167.9 GPa),⁸² we find that Al decreases the bulk modulus of Fe. This trend is well reproduced by the present theoretical results. For Fe-Cr, the agreement between theory and experiment⁴ is good, both of them showing minimum around 5 at. % Cr. For Fe-Mn, the theoretical slope resembles the average experimental slope below $x=0.05.$ On the other hand, the marked minimum in the theoretical $B(x)$ near 5 at. % Mn is completely absent from the measured trend. The reason for this discrepancy could be the low solu-

TABLE III. Theoretical (EMTO) bulk modulus $B(x)$ (in GPa) calculated for the ferromagnetic bcc $Fe_{1-x}M_x$ ($M=Al, Si, V, Cr, Mn, Co, Ni,$ and $Rh; 0 \leq x \leq 0.1$) random alloys. For pure Fe, the corresponding value is $B(0)=193.87$ GPa (Ref. 16).

x	$B(x)$							
	Fe-Al	Fe-Si	Fe-V	Fe-Cr	Fe-Mn	Fe-Co	Fe-Ni	Fe-Rh
0.025	175.59	179.20	187.90	182.35	176.24	188.25	176.67	187.20
0.05	164.43	172.73	184.00	177.88	169.99	184.04	163.29	181.84
0.075	156.55	170.45	182.03	179.30	173.52	181.15	153.55	177.87
0.1	152.47	171.33	183.21	181.24	181.78	179.19	148.90	173.57

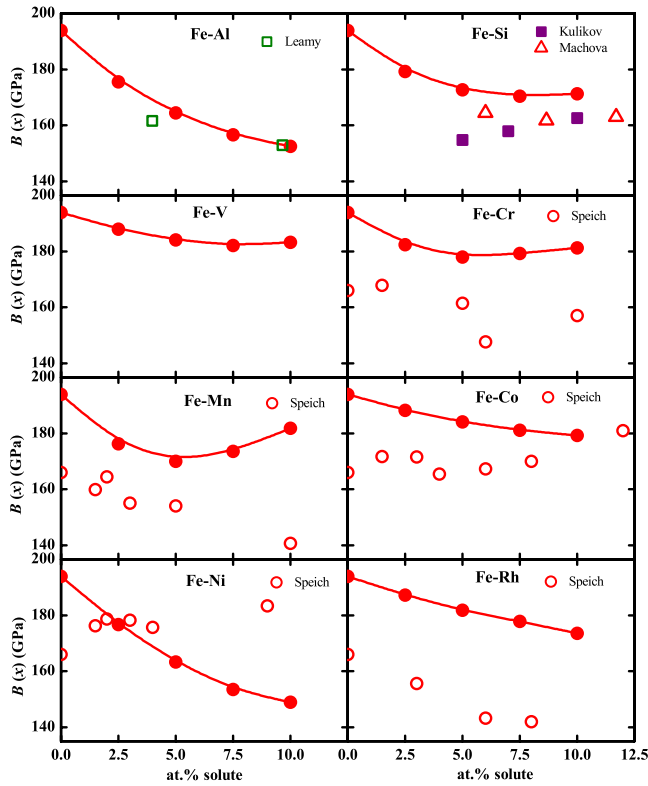


FIG. 6. (Color online) Theoretical (present results, solid circles connected with lines) bulk moduli of ferromagnetic bcc $\text{Fe}_{1-x}\text{M}_x$ ($M=\text{Al, Si, V, Cr, Mn, Co, Ni, and Rh}$; $0 \leq x \leq 0.1$) random alloys. Former theoretical results for Fe-Si (Ref. 74) (solid squares) and the available experimental data (Refs. 4 and 76) (open circles and triangles) are shown for comparison. The estimated bulk moduli for Fe-Al using the measured single-crystal elastic constants (Ref. 81 are also shown (open squares).

bility (up to 3 at. %) of Mn in α -Fe, which suggests that the experimental points at 5 and 10 at. % Mn already belong to the two-phase ($\alpha+\gamma$) region.⁴ The agreement for Fe-Rh is also satisfactory. Some inconsistencies can be seen between the theoretical and experimental data for Fe-Co and Fe-Ni. For the prior, experiment gives constant or slightly increasing slope at low concentrations,⁴ in contrast to the negative theoretical slope. Similar difference can be observed for the Fe-rich Fe-Ni alloys. It is tempting to lay the blame on the large theoretical size misfit parameters (Fig. 4) for these differences in the bulk modulus. However, in that situation for all binaries, the theoretical $dB(x)/dx$ value should be more negative than the experimental counterpart, which is not the case for Fe-Mn, Fe-Cr, and Fe-Rh.

For Fe-Si, previous theoretical results obtained for x between 0.05 and 0.1,⁷⁴ predict slightly increasing bulk modulus with Si content. The present theoretical $B(x)$ for Fe-Si, on the other hand, follows closely the available experimental data for 6–11.7 at. % Si.⁷⁶ Furthermore, combining the room-temperature experimental bulk modulus of Fe with those measured between 6 and 11.7 at. % Si,⁷⁶ one obtains that the bulk modulus of Fe-Si decreases with Si addition, which confirms our theoretical finding.

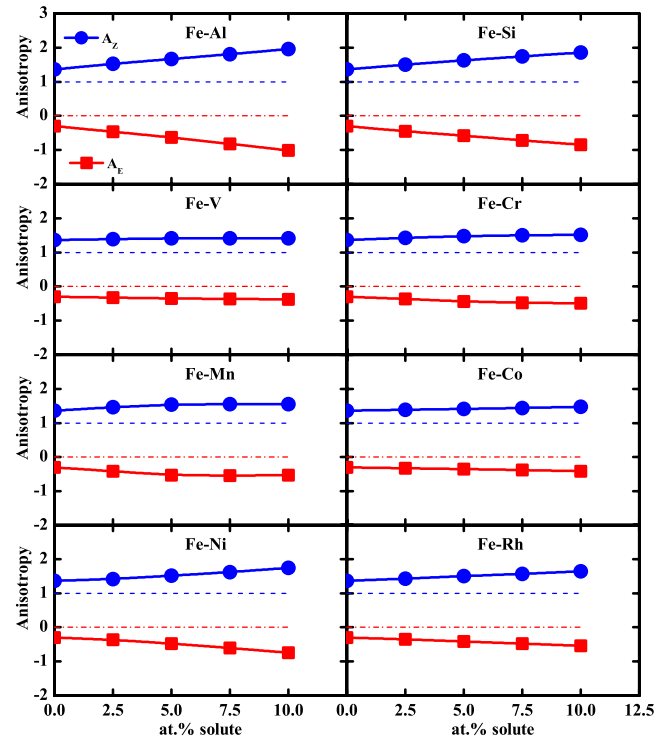


FIG. 7. (Color online) Theoretical (present results) Every (A_E , red squares connected with lines) and Zener (A_Z , blue circles connected with lines) anisotropy parameters of ferromagnetic bcc $\text{Fe}_{1-x}\text{M}_x$ ($M=\text{Al, Si, V, Cr, Mn, Co, Ni, and Rh}$; $0 \leq x \leq 0.1$) random alloys. The isotropic values are shown by red dashed-dotted (Every) and blue dashed (Zener) lines.

D. Elastic anisotropy

The present Every (A_E) and Zener (A_Z) anisotropy parameters for ferromagnetic bcc Fe are -0.3 and 1.37 , respectively. These ratios are different from the experimental values at 4 K (-1.14 and 2.32 , respectively⁸²) predicting significantly more isotropic lattice than the experiment. Since C_{12} and C_{44} are rather well reproduced by the theory,¹⁶ the above discrepancy between theory and experiment may be ascribed to the large theoretical C_{11} (and thus C'). We note that the experimental C_{11} in combination with the theoretical C_{12} and C_{44} , yields -1.0 and 2.37 for A_E and A_Z , respectively. Zhang *et al.* (Ref. 16) argued that about 50% of the error in the theoretical C_{11} is due to the underestimated equilibrium volume and the rest has a complex electronic structure and magnetic origin, which is not captured by the common density-functional approximation.

Next we study the variation in the anisotropy ratios with impurity concentration in bcc $\text{Fe}_{1-x}\text{M}_x$. As shown in Fig. 7, except for the slight local extremes at 7.5 at. % Mn, the individual A_E (A_Z) parameters decrease (increase) almost linearly with increasing x . That is, for all binaries considered here, the calculated anisotropy increases or remains nearly constant with alloying. Aluminum, silicon, and nickel increase the anisotropy of bcc Fe the most. For instance, 10 at. % Al enhances A_Z from 1.37 to 1.95 and decreases A_E from -0.3 to -1.0 . High elastic anisotropy was also reported in ordered ($B2$) Fe-Al alloys with 0.2–0.3 atomic fraction of

Al.⁸³ Chromium, manganese, and rhodium additions produce intermediate variations in A_E and A_Z whereas vanadium and cobalt leave the anisotropy parameters almost unchanged.

V. DISCUSSION

The calculated single-crystal elastic constants of $\text{Fe}_{1-x}M_x$ ($M=\text{Al, Si, V, Cr, Mn, Co, Ni, and Rh}$; $0 \leq x \leq 0.1$) random alloys follow a rather smooth composition dependence with some shallow local extremes around $x \approx 0.05$. Hence, parameterization of $C_{ij}(x)$ using simple functions (e.g., low-order polynomials) is possible. After such parameterization is made, our theoretical data from Fig. 5 (Table II) can be used as a consistent database for modeling the mechanical properties of Fe- M alloys at low temperature. The primary strength of such first-principles calculations, however, is to reveal the electronic origin of the alloying effects. There are several open questions regarding the calculated trends which could be answered using our electronic-structure data. One of the most surprising phenomena in Fig. 5 is the composition dependence of $C_{44}(x)$. The pressure derivatives of the elastic constants of Fe are all positive.⁸⁴ Therefore, since all alloying elements increase the lattice parameter of bcc Fe (Fig. 3), one would expect that they lower the single-crystal elastic constants. This is clearly not the case for C_{44} upon Al, Si, V, Cr, and Mn additions to Fe (Fig. 5). Here we try to find a possible reason behind this peculiar behavior. To this end, first we single out the volume effect on $\Delta C_{ij}/\Delta x$ and then investigate the effect of lattice distortion on the electronic structure of Fe and Fe- M alloys.

A. Volume effect on $\Delta C_{ij}(x)/\Delta x$

In Fig. 8, we compare the effect of volume expansion on $C_{ij}[(\Delta C_{ij}/\Delta x)_V]$ with the calculated total alloying effect $[\Delta C_{ij}/\Delta x]$. The volume effect was estimated from the volume dependence of C_{ij} for bcc Fe [dC_{ij}/dV] and the volume change caused by alloying (dV/dx), viz.,

$$\left(\frac{\Delta C_{ij}}{\Delta x}\right)_V \equiv \frac{dC_{ij}}{dV} \times \frac{dV}{dx}. \quad (3)$$

Here dC_{ij}/dV is the numerical derivative of C_{ij} calculated for pure bcc Fe for five different volumes around the theoretical equilibrium volume, and dV/dx was obtained from the average slope of $a(x)$ between $0 \leq x \leq 0.05$ (Fig. 3). The volume effect is shown by empty symbol in Fig. 8. The total alloying effects, $\Delta C_{ij}/\Delta x$, were derived from the average slopes of $C_{ij}(x)$ between $0 \leq x \leq 0.05$ (Fig. 5) and they are shown by solid symbol in Fig. 8.

It is found that for the tetragonal elastic constant C' , the estimated $(\Delta C'/\Delta x)_V$ resembles rather well the total alloying effects. Exceptions are Fe-Al and Fe-Si but even for these two systems $(\Delta C'/\Delta x)_V$ can account for only about 40% and 30% of $\Delta C'/\Delta x$. The largest volume effects are obtained for Al and Rh (Fig. 4), which also give the largest $\Delta C'/\Delta x$ values. On the other hand, in the case of Fe-Al, Fe-Si, Fe-V, Fe-Cr, and Fe-Mn, the volume effect $(\Delta C_{44}/\Delta x)_V$ has a sign opposite to that obtained for $\Delta C_{44}/\Delta x$. Furthermore, for all elements $(\Delta C_{44}/\Delta x)_V < \Delta C_{44}/\Delta x$ whereas for C' , there is no

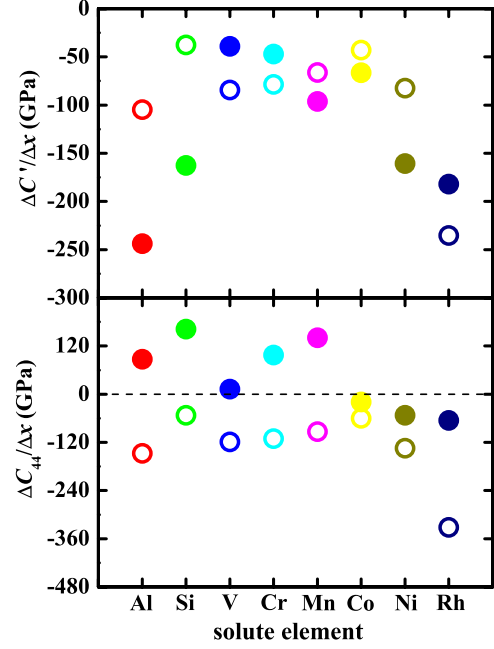


FIG. 8. (Color online) Comparison between the volume expansion effect $(\Delta C_{ij}/\Delta x)_V$ (in GPa per atomic fraction, open circles) and total alloying effect $\Delta C_{ij}/\Delta x$ (in GPa per atomic fraction, filled circles) on C' (upper panel) and C_{44} (lower panel) elastic constants of ferromagnetic bcc $\text{Fe}_{0.95}M_{0.05}$ ($M=\text{Al, Si, V, Cr, Mn, Co, Ni, and Rh}$) random alloys.

clear trend in the sign of $(\Delta C'/\Delta x)_V - \Delta C'/\Delta x$. It follows that the composition dependence of $C_{44}(x)$ is governed by electronic (magnetic) effects other than the simple alloying induced volume change. These complex electronic mechanisms seem to be strong enough to overwrite the volume effects on $C_{44}(x)$.

B. Electronic-structure effects on $C_{44}(x)$

An elastic constant C is defined as the second-order derivative of the total energy $E(\delta) = E(0) + a\delta^2 + O(\delta^4)$ [where $O(\delta^4)$ stands for the neglected terms] calculated as a function of the distortion parameter δ . Since usually δ is very small (< 0.05), one can neglect the higher-order terms in δ obtaining $C \sim \Delta E(\delta)/\delta^2$, where $\Delta E(\delta) \equiv E(\delta) - E(0)$ represents the change in the total energy upon lattice distortion. Thus by tracing the composition dependence of $\Delta E(\delta)$, one can also understand the behavior of C . The total-energy change, in turn, may be expressed as the sum of the changes in the kinetic, Hartree, and exchange-correlation energies. According to the force theorem,^{85,86} the leading term in the total-energy difference ΔE is the band-energy part of the kinetic energy ΔE_b . In our case, we have

$$\Delta E_b(\delta) \equiv \int^{\varepsilon_F} \varepsilon [N(\varepsilon, \delta) - N(\varepsilon, 0)] d\varepsilon, \quad (4)$$

where $N(\varepsilon, \delta)$ is the density of states (DOS) for energy ε and lattice distortion δ , and the integral includes all states below the Fermi level ε_F . In solids with small or constant DOS around ε_F , $N(\varepsilon, \delta)$ shows weak δ (i.e., lattice distortion) de-

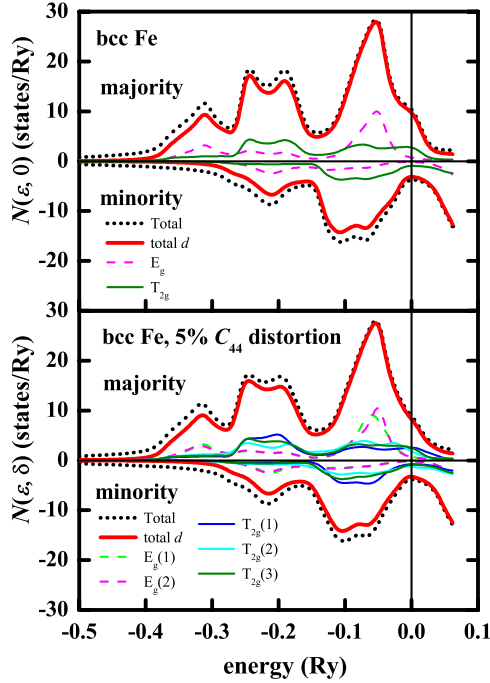


FIG. 9. (Color online) Total (black thick dotted lines), partial d (red thick solid lines), and partial T_{2g} (color thin solid lines) and E_g (color thin dashed lines) density of states of bcc Fe without lattice distortion (upper panel) and with 5% distortion used to calculate the C_{44} elastic constant (lower panel). The figure illustrates how T_{2g} and E_g bands are split by lattice distortion. The energy scale is set relative to the Fermi level.

pendence and thus the band-energy contribution to $\Delta E(\delta)$ (and thus to the elastic constant C) is negligible. However, in metals with a large DOS peak at ϵ_F , the situation may be quite different. Lattice distortion may significantly alter $N(\epsilon, \delta)$ by splitting the DOS peak at ϵ_F . As a consequence, the band energy lowers, which gives a negative contribution to $\Delta E(\delta)$ and to C . In such cases, the elastic constant corresponding to the particular lattice distortion remains positive only if the rest of $\Delta E(\delta)$ (mainly the electrostatic term) is

large enough to cancel the negative $\Delta E_b(\delta)$. Here we will show that the above scenario occurs also in ferromagnetic bcc Fe when a monoclinic C_{44} distortion is applied.

The density of states of Fe and Fe-based binary random alloys were computed at their equilibrium volumes. Figure 9 displays the total (thick dotted lines) and the partial d (thick solid lines) DOS of pure Fe: $N(\epsilon, 0)$ is for the bcc lattice (upper panel) and $N(\epsilon, \delta)$ is for a distorted lattice ($\delta=0.05$) corresponding to the C_{44} elastic constant (lower panel). Since for Fe, the d band dominates the shape of the DOS, in the following we focus only on the d DOS. In cubic environment, the d band is formed by the triple-degenerated T_{2g} band and by the double-degenerated E_g band. In Fig. 9, these two subbands are shown by thin solid lines (T_{2g}) and thin dashed lines (E_g). In Table IV, we list the present $N(\epsilon_F, \delta)$ values for the T_{2g} and E_g bands, for both the majority (\uparrow) and the minority (\downarrow) spin channels, and for $\delta=0$ and $\delta=0.05$.

The majority channel [$N^\uparrow(\epsilon, 0)$] of bcc Fe (Fig. 9, upper panel) is almost completely saturated and the minority channel [$N^\downarrow(\epsilon, 0)$] has filled bonding and empty antibonding states. The Fermi level in the minority band is pinned to the pseudogap separating the bonding and antibonding states with rather small and smooth $N^\downarrow(\epsilon, 0)$ around ϵ_F . Therefore, no substantial changes are expected in $N^\downarrow(\epsilon, \delta)$ upon lattice distortion. On the other hand, in the majority band, $N^\uparrow(\epsilon, 0)$ is large and has a pronounced shoulder at ϵ_F . Decomposing $N^\uparrow(\epsilon, 0)$ into T_{2g} and E_g components, we find that the shoulder at ϵ_F has almost pure T_{2g} character. Therefore, lattice distortion should have a marked effect on this subband. Indeed, $\delta=0.05$ C_{44} distortion (Fig. 9, lower panel) splits the triple-degenerated T_{2g}^\uparrow band in such a way that two out of the three bands are shifted toward negative energies. This shift is reflected in a large drop of the total T_{2g}^\uparrow DOS at the Fermi level, viz., $\Delta N^\uparrow(\epsilon_F, \delta) \equiv N^\uparrow(\epsilon_F, \delta) - N^\uparrow(\epsilon_F, 0) \approx -1.4$ states/Ry. For comparison, the same lattice distortion for the minority T_{2g}^\downarrow channel gives $N^\downarrow(\epsilon_F, \delta) - N^\downarrow(\epsilon_F, 0) \approx 0.04$ states/Ry. The distortion-induced shift moves the weight of the majority T_{2g}^\uparrow band toward lower energies resulting in $\Delta E_b(\delta) < 0$. Note that in ferromagnetic bcc Fe,

TABLE IV. The partial T_{2g} and E_g DOS (states/Ry) of ferromagnetic bcc Fe and $\text{Fe}_{0.95}\text{M}_{0.05}$ ($M=\text{Al, Si, V, Cr, Mn, Co, Ni, and Rh}$) random alloys without and with 5% C_{44} distortion. Listed are also the C_{44} values (in GPa) for $\text{Fe}_{0.95}\text{M}_{0.05}$ relative to that of pure Fe. For alloys, the average DOS values are shown.

System	No distortion				5% C_{44} distortion				ΔC_{44}
	T_{2g}^\uparrow	T_{2g}^\downarrow	E_g^\uparrow	E_g^\downarrow	T_{2g}^\uparrow	T_{2g}^\downarrow	E_g^\uparrow	E_g^\downarrow	
Pure Fe	8.268	2.853	1.448	0.302	6.839	2.890	1.403	0.382	
Fe-Al	6.942	3.756	1.404	0.664	5.866	3.643	1.367	0.749	4.61
Fe-Si	6.654	3.600	1.328	0.658	5.657	3.502	1.299	0.732	8.42
Fe-V	6.225	2.859	1.378	0.314	5.221	2.917	1.334	0.402	1.13
Fe-Cr	5.718	2.940	1.416	0.384	4.949	3.074	1.415	0.490	6.10
Fe-Mn	6.282	3.138	2.116	0.552	5.674	3.225	2.173	0.617	8.00
Fe-Co	7.614	2.991	1.256	0.352	6.205	3.034	1.191	0.457	-0.58
Fe-Ni	6.993	3.879	1.638	0.628	5.817	3.795	1.582	0.736	-2.14
Fe-Rh	6.966	3.246	1.200	0.370	5.782	3.168	1.152	0.481	-2.37

there must be large positive electrostatic (plus exchange-correlation) contribution (not shown) which compensates the above band-energy change and leads to positive $\Delta E(\delta)$ and positive C_{44} (106.73 GPa). Based on the above mechanism, we propose that those alloying additions which significantly alter the majority T_{2g}^\uparrow peak of bcc Fe also enhance the C_{44} elastic constant of Fe. However, this enhancement may to some extent be cancelled by the negative volume effect.

From the present DOS results listed in Table IV, one finds that all alloying additions considered here lower the size of the total (average) T_{2g}^\uparrow DOS at the Fermi level. Thus, we can anticipate that these solute elements also have a corresponding impact on the C_{44} elastic constant of bcc Fe. Aluminum, silicon, vanadium, chromium, and manganese modify the electronic structure in such a way that the change in the T_{2g}^\uparrow DOS upon C_{44} lattice distortion becomes $\Delta N^\uparrow(\varepsilon_F, \delta) > -1.0$ states/Ry (compared to -1.4 states/Ry obtained for pure Fe). This means that the negative band-energy contribution to $\Delta E(\delta)$ and to C_{44} is reduced by these alloying elements. That is, from electronic-structure considerations Al, Si, V, Cr, and Mn are expected to increase C_{44} . This is in perfect agreement with Fig. 5 and Table II (see also the last column in Table IV). In particular, 5% Si, Cr, and Mn increase $\Delta N^\uparrow(\varepsilon_F, \delta)$ to -0.99 , -0.77 , and -0.61 states/Ry and increase C_{44} of bcc Fe by 8.4 GPa, 6.1 GPa, and 8.0 GPa, respectively. The reason why Si yields the largest change on C_{44} is that this element produces the smallest (negative) volume effect. Vanadium, on the other hand, has a large volume term (Fig. 8), which effectively reduces the electronic-structure-driven enhancement of C_{44} .

Cobalt leaves the total T_{2g}^\uparrow DOS change almost intact, giving $\Delta N^\uparrow(\varepsilon_F, \delta) \approx -1.4$ states/Ry (Table IV). The volume effect of Co is also small (Fig. 8), which explains the nearly vanishing Co effect on C_{44} of bcc Fe. Nickel and rhodium slightly reduce the T_{2g}^\uparrow DOS change in bcc Fe, both of them giving $\Delta N^\uparrow(\varepsilon_F, \delta) \approx -1.2$ states/Ry. Accordingly, these two elements also produce an electronic-structure-driven enhancement of C_{44} . On the other hand, since they increase the lattice parameter of bcc Fe rather significantly, the total Ni and Rh alloying effects on C_{44} will remain close to zero.

The proposed volume plus electronic-structure mechanism gives a simple qualitative picture of the alloying effects on C_{44} of bcc Fe. However, there are also some exceptions which do not completely follow the expected trends. For instance, in spite of the fact that Ni and Rh produce similar

$\Delta N^\uparrow(\varepsilon_F, \delta)$ but different volume effects, their total alloying effects on C_{44} are very close to each other. It is clear that other complex mechanisms are needed for a more accurate model of the alloying effects on the elastic constants of ferromagnetic bcc Fe. This is the topic of further research.

VI. CONCLUSIONS

The elastic properties of ferromagnetic bcc $\text{Fe}_{1-x}\text{M}_x$ ($M = \text{Al, Si, V, Cr, Mn, Co, Ni, and Rh}$; $0 \leq x \leq 0.1$) random alloys have been investigated using the EMTO method in combination with the coherent-potential approximation. In general, the calculated single-crystal elastic constants for Fe-Al and the bulk moduli for all binaries show good agreement with the available experimental data. All solute atoms enlarge the lattice parameter and decrease the C_{11} , C_{12} , and C' single-crystal elastic constants of bcc Fe. At the same time, nearly constant or slightly increasing trends are obtained for $C_{44}(x)$. This anomalous behavior is explained using the electronic structure of ferromagnetic bcc Fe and Fe- M alloys. On the average, the most significant alloying effects on the single-crystal elastic constants appear when Al, Si, or Ni is added to bcc Fe. The anisotropy is found to be enhanced by Al, Si, and Ni additions, compared to that of pure bcc Fe.

The present theoretical data may serve as a consistent starting point for modeling the mechanical properties of Fe-based alloys. The few discrepancies found between the calculated and the measured data call for further improvements in the theoretical approach, e.g., by accounting for the temperature effects. In addition, more accurate measurements of the elastic properties of ferromagnetic Fe-based alloys by employing modern experimental techniques would be desired.

ACKNOWLEDGMENTS

The Swedish Research Council, the Swedish Foundation for Strategic Research, the Swedish Energy Agency, the Swedish Iron Office (Jernkontoret), the Carl Tryggers Foundation, and the China Scholarship Council are acknowledged for financial support. Part of the calculations was performed using the facilities of the Finnish Centre for Scientific Computing (CSC).

¹A. S. Aragon, S. Backer, F. A. McClintock, G. S. Reichenbach, E. Orowan, M. C. Shaw, and E. Rabinowicz, *Metallurgy and Materials* (Addison-Wesley, Ontario, 1966).

²C. W. Lung and N. H. March, *Mechanical Properties of Metals: Atomistic and Fractal Continuum Approaches* (World Scientific, Singapore, 1999).

³S. Takeuchi, *J. Phys. Soc. Jpn.* **27**, 929 (1969).

⁴G. R. Speich, A. J. Schwobele, and W. C. Leslie, *Metall. Trans.* **3**, 2031 (1972).

⁵K. Okazaki, *J. Mater. Sci.* **31**, 1087 (1996).

⁶G. Ghosh and G. B. Olson, *Acta Mater.* **50**, 2655 (2002).

⁷R. L. Fleischer, *Acta Metall.* **11**, 203 (1963).

⁸R. Labusch, *Acta Metall.* **20**, 917 (1972).

⁹F. R. N. Nabarro, *Philos. Mag.* **35**, 613 (1977).

¹⁰J. Crangle and G. C. Hallam, *Proc. R. Soc. London* **272**, 119 (1962).

¹¹P. James, O. Eriksson, B. Johansson, and I. A. Abrikosov, *Phys. Rev. B* **59**, 419 (1999).

¹²A. M. N. Niklasson, B. Johansson, and H. L. Skriver, *Phys. Rev. B* **59**, 6373 (1999).

- ¹³S. Ghosh, B. Sanyal, C. B. Chaudhuri, and A. Mookerjee, *Eur. Phys. J. B* **23**, 455 (2001).
- ¹⁴K. Schwarz and D. R. Salahub, *Phys. Rev. B* **25**, 3427 (1982).
- ¹⁵P. A. Korzhavyi, A. V. Ruban, J. Odqvist, J.-O. Nilsson, and B. Johansson, *Phys. Rev. B* **79**, 054202 (2009).
- ¹⁶H. L. Zhang, B. Johansson, and L. Vitos, *Phys. Rev. B* **79**, 224201 (2009).
- ¹⁷P. Olsson, I. A. Abrikosov, L. Vitos, and J. Wallenius, *J. Nucl. Mater.* **321**, 84 (2003).
- ¹⁸O. K. Andersen, O. Jepsen, and G. Krier, in *Lectures on Methods of Electronic Structure Calculations*, edited by V. Kumar, O. K. Andersen, and A. Mookerjee (World Scientific, Singapore, 1994), p. 63.
- ¹⁹L. Vitos, *Phys. Rev. B* **64**, 014107 (2001).
- ²⁰L. Vitos, I. A. Abrikosov, and B. Johansson, *Phys. Rev. Lett.* **87**, 156401 (2001).
- ²¹P. Soven, *Phys. Rev.* **156**, 809 (1967).
- ²²B. L. Györfy, *Phys. Rev. B* **5**, 2382 (1972).
- ²³O. Kubaschewski, *Iron-Binary Phase Diagrams* (Springer, Berlin, 1982).
- ²⁴T. B. Massalski, *Binary Alloy Phase Diagrams* (American Society for Metals, Metals Park, Ohio, 1986).
- ²⁵M. C. M. Farquhar, H. Lipson, and A. R. Weill, *J. Iron Steel Inst. London* **152**, 457 (1945).
- ²⁶F. Lihl and H. Ebel, *Arch. Eisenhuettenwes.* **32**, 489 (1961).
- ²⁷E. P. Elsukov, G. N. Konygin, V. A. Barinov, and E. V. Voronina, *J. Phys.: Condens. Matter* **4**, 7597 (1992).
- ²⁸P. Olsson, I. A. Abrikosov, and J. Wallenius, *Phys. Rev. B* **73**, 104416 (2006).
- ²⁹M. Ropo, K. Kokko, M. P. J. Punkkinen, S. Hogmark, J. Kollár, B. Johansson, and L. Vitos, *Phys. Rev. B* **76**, 220401 (2007).
- ³⁰G. Kresse and J. Furthmüller, *Comput. Mater. Sci.* **6**, 15 (1996).
- ³¹G. Kresse and J. Furthmüller, *Phys. Rev. B* **54**, 11169 (1996).
- ³²G. Kresse and J. Hafner, *Phys. Rev. B* **47**, 558 (1993).
- ³³G. Kresse and J. Hafner, *Phys. Rev. B* **49**, 14251 (1994).
- ³⁴P. Hohenberg and W. Kohn, *Phys. Rev.* **136**, B864 (1964).
- ³⁵J. P. Perdew, K. Burke, and M. Ernzerhof, *Phys. Rev. Lett.* **77**, 3865 (1996).
- ³⁶W. Kohn and L. J. Sham, *Phys. Rev.* **140**, A1133 (1965).
- ³⁷J. Kollár, L. Vitos, and H. L. Skriver, in *Electronic Structure and Physical Properties of Solids: the Uses of the LMTO Method*, Lectures Notes in Physics, edited by H. Dreyssé (Springer-Verlag, Berlin, 2000), p. 85.
- ³⁸L. Vitos, H. L. Skriver, and B. Johansson, *Comput. Mater. Sci.* **18**, 24 (2000).
- ³⁹L. Vitos, *Computational Quantum Mechanicals for Materials Engineers* (Springer-Verlag, London, 2007).
- ⁴⁰L. Vitos, P. A. Korzhavyi, and B. Johansson, *Phys. Rev. Lett.* **88**, 155501 (2002).
- ⁴¹L. Dubrovinsky, N. Dubrovinskaia, F. Langenhorst, D. Dobson, D. Rubie, C. Geßmann, I. A. Abrikosov, B. Johansson, V. I. Baykov, L. Vitos, T. Le Bihan, W. A. Crichton, V. Dmitriev, and H.-P. Weber, *Nature (London)* **422**, 58 (2003).
- ⁴²L. Vitos, P. A. Korzhavyi, and B. Johansson, *Nature Mater.* **2**, 25 (2003).
- ⁴³N. Dubrovinskaia, L. Dubrovinsky, I. Kantor, W. A. Crichton, V. Dmitriev, V. Prakapenka, G. Shen, L. Vitos, R. Ahuja, B. Johansson, and I. A. Abrikosov, *Phys. Rev. Lett.* **95**, 245502 (2005).
- ⁴⁴A. E. Kissavos, S. I. Simak, P. Olsson, L. Vitos, and I. A. Abrikosov, *Comput. Mater. Sci.* **35**, 1 (2006).
- ⁴⁵L. Vitos, P. A. Korzhavyi, and B. Johansson, *Phys. Rev. Lett.* **96**, 117210 (2006).
- ⁴⁶B. Magyari-Köpe, G. Grimvall, and L. Vitos, *Phys. Rev. B* **66**, 064210 (2002).
- ⁴⁷B. Magyari-Köpe, L. Vitos, and G. Grimvall, *Phys. Rev. B* **70**, 052102 (2004).
- ⁴⁸A. Taga, L. Vitos, B. Johansson, and G. Grimvall, *Phys. Rev. B* **71**, 014201 (2005).
- ⁴⁹L. Huang, L. Vitos, S. K. Kwon, B. Johansson, and R. Ahuja, *Phys. Rev. B* **73**, 104203 (2006).
- ⁵⁰J. Zander, R. Sandström, and L. Vitos, *Comput. Mater. Sci.* **41**, 86 (2007).
- ⁵¹B. Magyari-Köpe, L. Vitos, B. Johansson, and J. Kollár, *Acta Crystallogr., Sect. B: Struct. Sci.* **57**, 491 (2001).
- ⁵²A. Landa, C.-C. Chang, P. N. Kumta, L. Vitos, and I. A. Abrikosov, *Solid State Ion.* **149**, 209 (2002).
- ⁵³B. Magyari-Köpe, L. Vitos, G. Grimvall, B. Johansson, and J. Kollár, *Phys. Rev. B* **65**, 193107 (2002).
- ⁵⁴B. Magyari-Köpe, L. Vitos, B. Johansson, and J. Kollár, *Geophys. Res.—Solid Earth* **107**, 2136 (2002).
- ⁵⁵G. A. Alers and J. R. Neighbours, *J. Appl. Phys.* **28**, 1514 (1957).
- ⁵⁶A. G. Every, *Phys. Rev. B* **22**, 1746 (1980).
- ⁵⁷C. Zener, *Elasticity and Anelasticity of Metals* (University of Chicago Press, Chicago, 1948).
- ⁵⁸V. L. Moruzzi, J. F. Janak, and K. Schwarz, *Phys. Rev. B* **37**, 790 (1988).
- ⁵⁹P. A. Korzhavyi, A. V. Ruban, I. A. Abrikosov, and H. L. Skriver, *Phys. Rev. B* **51**, 5773 (1995).
- ⁶⁰A. Zunger, S.-H. Wei, L. G. Ferreira, and J. E. Bernard, *Phys. Rev. Lett.* **65**, 353 (1990).
- ⁶¹L. Vitos, P. A. Korzhavyi, and B. Johansson, *Mater. Today* **5**, 14 (2002).
- ⁶²P. E. Blöchl, *Phys. Rev. B* **50**, 17953 (1994).
- ⁶³G. Kresse and D. Joubert, *Phys. Rev. B* **59**, 1758 (1999).
- ⁶⁴W. B. Pearson, *A Handbook of Lattice Spacings and Structures of Metals and Alloys* (Pergamon Press, Belfast, 1958).
- ⁶⁵A. J. Bradley and A. H. Jay, *J. Iron Steel Inst.* **125**, 339 (1932).
- ⁶⁶L. Sutton and W. Hume-Rothery, *Philos. Mag.* **46**, 1295 (1955).
- ⁶⁷A. R. Troiano and F. T. McGuire, *Trans. Am. Soc. Met.* **31**, 340 (1943).
- ⁶⁸A. P. Guljaev and E. F. Trusova, *Ž. Tekh. Fiz. SSSR* **20**, 66 (1950).
- ⁶⁹F. M. Walters and C. Wells, *Trans. Am. Soc. Met.* **23**, 727 (1935).
- ⁷⁰J. W. Rodgers and W. R. Maddocks, *Iron and Steel Inst. Spec. Rep.* **24**, 167 (1939).
- ⁷¹A. J. Bradley, A. H. Jay, and A. Taylor, *Philos. Mag.* **23**, 545 (1937).
- ⁷²E. A. Owen and E. L. Yates, *Proc. Phys. Soc. London* **49**, 307 (1937).
- ⁷³D. Oleszak and H. Matyja, *Nanostruct. Mater.* **6**, 425 (1995).
- ⁷⁴N. I. Kulikov, D. Fristot, J. Hugel, and A. V. Postnikov, *Phys. Rev. B* **66**, 014206 (2002).
- ⁷⁵N. I. Kulikov, D. Fristot, A. Postnikov, and J. Hugel, *Comput. Mater. Sci.* **17**, 196 (2000).
- ⁷⁶A. Machova and A. Kadeckova, *Czech. J. Phys. Sect. B* **27**, 555 (1977).
- ⁷⁷L. Vitos and B. Johansson, *Applied Parallel Computing, State of*

- the Art in Scientific Computing*, Lecture Notes in Computer Science, edited by B. Kagström *et al.* (Springer-Verlag, Berlin, 2007), p. 510.
- ⁷⁸M. Ropo, K. Kokko, and L. Vitos, *Phys. Rev. B* **77**, 195445 (2008).
- ⁷⁹L. Vitos, B. Johansson, J. Kollar, and H. L. Skriver, *Phys. Rev. B* **62**, 10046 (2000).
- ⁸⁰G. I. Csonka, J. P. Perdew, A. Ruzsinszky, P. H. T. Philipsen, S. Lebègue, J. Paier, O. A. Vydrov, and J. G. Ángyán, *Phys. Rev. B* **79**, 155107 (2009).
- ⁸¹H. J. Leamy, E. D. Gibson, and F. X. Kayser, *Acta Metall.* **15**, 1827 (1967).
- ⁸²J. E. Rayne and B. S. Chandrasekhar, *Phys. Rev.* **122**, 1714 (1961).
- ⁸³R. G. V. D. Heide and S. M. Allen, *Acta Mater.* **44**, 1613 (1996).
- ⁸⁴G. Simmons and H. Wang, *Single Crystal Elastic Constants and Calculated Aggregate Properties* (MIT Press, Cambridge, MA, 1971).
- ⁸⁵H. L. Skriver, *Phys. Rev. B* **31**, 1909 (1985).
- ⁸⁶A. R. Mackintosh and O. K. Andersen, *Electrons at the Fermi Surface* (Cambridge University Press, Cambridge, 1980).